EGSnrc Monte Carlo calculated dosimetry parameters for ^{192}Ir and ^{169}Yb brachytherapy sources

R. E. P. Taylor[a] and D. W. O. Rogers[b]
Carleton Laboratory for Radiotherapy Physics, Ottawa Carleton Institute of Physics, Carleton University Campus Ottawa, Ontario K1S 5B6, Canada

(Received 25 June 2008; revised 21 August 2008; accepted for publication 31 August 2008; published 14 October 2008)

This study presents the results of EGSnrc Monte Carlo calculations of the dose distribution surrounding a high dose rate ^{169}Yb brachytherapy source and 14 high dose rate and pulsed dose rate ^{192}Ir brachytherapy sources. Energy-weighted spectra of emitted photons, a full set of TG-43 dosimetry parameters, along-away dose tables, and a description of the materials and geometry used for each source are provided. In addition to this, separate tallies are made of the dose contributed from primary, single-scattered, and multiply-scattered photons. Separation of dose in this manner allows one to use convolution/superposition methods to calculate the dose surrounding a brachytherapy source accounting for a non-homogeneous medium. The effect of phantom size on TG-43 dosimetry parameters and scattered dose is also investigated for the ^{192}Ir microSelectron v2 HDR source. This paper describes the calculation methods and presents the dose rate constants calculated for each source with the full set of dosimetry data being available online at the Carleton Laboratory for Radiotherapy Physics brachytherapy database (http://www.physics.carleton.ca/clrp/seed_database/). © *2008 American Association of Physicists in Medicine*. [DOI: 10.1118/1.2987676]

Key words: brachytherapy, ^{192}Ir, ^{169}Yb, EGSnrc, Monte Carlo, primary scatter separated dose, database, high dose rate, pulsed dose rate

I. INTRODUCTION

Our group recently published[1] a comprehensive set of Monte Carlo (MC) calculated TG-43[2–4] dosimetry parameters for 27 ^{125}I and ^{103}Pd brachytherapy sources used in permanent implant and eye plaque treatments. All of the data from that study are currently available online via the Carleton Laboratory for Radiotherapy Physics website at http://www.physics.carleton.ca/clrp/seed_database/. One of our goals for this website is to make it a more complete resource by including data for other brachytherapy modalities and isotopes. To that end, this study presents the results of MC calculations performed for a high dose rate (HDR) ^{169}Yb source and 14 HDR and pulsed dose rate (PDR) ^{192}Ir sources using the EGSnrc[5,6] user-code BrachyDose.[7,8] Included in these calculations are a complete set of TG-43 dosimetry parameters, along-away dose tables (described in Sec. II C), primary and scatter dose components separated as described below, and energy-weighted photon spectra useful, for example, to calculate dose surrounding brachytherapy sources using primary and scatter dose separation (PSS) models.[9]

As an alternative to the TG-43 dosimetry protocol, and MC calculations, convolution/superposition methods can also be used to calculate the doses surrounding brachytherapy sources.[10–15] The primary dose can also act as the source descriptor for scatter dose calculations according to the primary and scatter dose separation (PSS) formalism described by Russell *et al.*[9] The goal of using superposition methods is to use contributions from primary and scatter doses to account for inhomogeneities or the lack of a full scattering medium, which are ignored by the TG-43 protocol. In this study, primary, total scatter, single scatter, and multiple scatter dose are calculated and tabulated for all sources. The effect of phantom size on scatter contribution to dose and TG-43 dosimetry parameters is also investigated for the ^{192}Ir microSelectron v2 HDR source.

Due to the large volume of data associated with this study, the complete set of dosimetry parameters is not presented here. Instead, only the geometry descriptions and calculated dose rate constants for each source, along with dose rate constants previously reported by other authors, are presented in this paper and cases of significant discrepancies between the current and previous calculations are noted. The complete dataset is available online via the CLRP website.

II. METHODS AND MONTE CARLO MODELS

II.A. Brachytherapy sources

For this study Yegin's multi-geometry package[16] is used to model source geometries as carefully as possible based on the information presented by authors of previous publications. Geometry models include source encapsulation, internal source geometry, the distribution of radioactivity within the source, and the stainless steel cable connected to the sources for use in after-loading systems. Descriptions of the source geometries used in this study are provided below and are also available with to-scale drawings, as part of the web resource.

II.B. Monte Carlo calculations

The Monte Carlo methods for calculations in this study are described in detail by Taylor *et al.*[8,1] and, as such, are only briefly described here. BrachyDose scores the collision kerma per history in a geometric region (voxel) via a track-length estimator (described in Ref. 8). Studies by a number of authors have shown that for distances less than 0.2 cm from the central axis of an ^{192}Ir source, photon tracklength estimators do not provide an accurate estimate of the true dose.[17–21] A study by Wang and Li[18] concluded that the track-length estimator is not accurate near the source ($r \leq 0.2$ cm) because electronic equilibrium may not exist and the dose contribution from the beta spectrum of ^{192}Ir (average energy of 181 keV) is ignored. Wang and Li showed that, for the VariSource classic, the dose scored by energy deposition (including dose from the ^{192}Ir beta spectrum) may be greater than the tracklength-estimated dose by as much as 29% and 7% at distances from the center of the source of $r=0.05$ cm and $r=0.1$ cm, respectively[18] (0.02 and 0.07 cm from the source encapsulation). At a distance of 0.2 cm from the center of the source this difference drops to 1% or less. Ignoring the contribution from the ^{192}Ir beta spectrum, Wang and Li calculated that for the VariSource classic the dose from photons (as opposed to betas and photons) scored via energy deposition is 7.4% and 3.2% greater than the tracklength-estimated dose at distances from the center of the source of $r=0.05$ cm and $r=0.1$ cm, respectively. This is consistent with our calculations as demonstrated by Fig. 1(a), which plots the ratio of dose scored using energy deposition (i.e., when transporting electrons down to 1 keV) to dose scored using the tracklength estimator (with no electron transport) as a function of distance from the center of the source along the transverse axis for the VariSource classic and microSelectron v2 sources. Figure 1(b) shows the dose to kerma ratio along the transverse axis calculated for the ^{169}Yb HDR 4140. For the HDR 4140, the tracklength estimator underestimates the dose by 16% at 0.06 cm from the center of the source, however, this difference drops to $<1\%$ at a distance of 0.09 cm from the center of the source. Along the seed axis of the microSelectron v2, the dose scored using energy deposition is roughly 1% greater than the kerma at a distance of 0.1 cm from the source encapsulation ($r=0.3$ cm). This difference drops to less than 0.3% at a distance of 0.3 cm from the source encapsulation ($r=0.5$ cm) along the seed axis. As Wang and Li noted, the difference between dose scored using energy deposition and tracklength estimators depends on the source geometry and materials.[18] Since electron transport is not done for this study, dosimetry parameters are not reported for distances less than 0.2 cm from the source encapsulation. Also, since electrons are not transported, the 0.2%–0.3% contribution to air kerma strength from bremsstrahlung photons originating in the source is not accounted for in these calculations.[22]

For the transport of photons, Rayleigh scattering, bound Compton scattering, photo-electric absorption and fluorescent emission of characteristic x rays are all simulated. The photon cutoff energy is set to 1 keV for all dose to water calculations. Photon cross sections from the XCOM (Ref. 23) database are used and mass-energy absorption coefficients are calculated using the EGSnrc user-code "g." The incident ^{192}Ir spectrum (average energy of ~370 keV) used in this study is taken from work by Duchemin and Coursol[24] (see also work by Borg and Rogers[22]) while the ^{169}Yb spectrum (average energy of ~93 keV) is the simplified spectrum presented by Medich *et al.*[25]

Dose calculations are performed with the source positioned at the center of a rectilinear water phantom (mass density of 0.998 g/cm^3) with dimensions of $80\times80\times80$ cm^3, which is an effectively infinite scattering medium for distances up to 20 cm from the center of an ^{192}Ir or ^{169}Yb source.[26,27] Dose distributions surrounding the source are

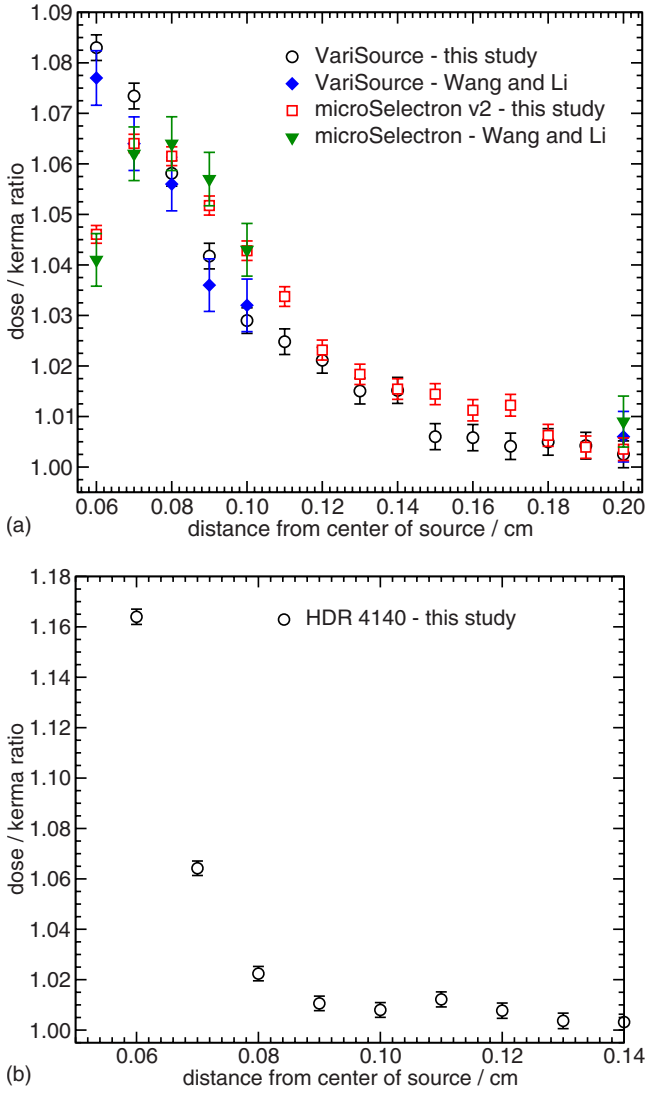

FIG. 1. Ratio of dose, along the transverse axis, from the source photons only scored using energy deposition (with electron transport down to 1 keV) to dose scored using a tracklength estimator (kerma) for (a) ^{192}Ir VariSource classic and microSelectron v2 and (b) ^{169}Yb HDR 4140. The radius of the encapsulation for these three sources is 0.030, 0.045, and 0.045 cm, respectively. The ^{192}Ir data calculated in this study are compared with the values calculated by Wang and Li (Ref. 18).

scored in a two-dimensional grid of cubic voxels located on a plane defined by the source axis (z-axis) and the transverse axis (x-axis). To take advantage of the simulation symmetry, doses from either side of the source axis in the xz-plane are averaged. Uncertainties on the average doses are calculated using the approximation that the dose in these two halves of the plane are statistically independent. To minimize the impact of voxel size effects[8,28,29] while maintaining reasonable efficiency, voxel sizes are chosen in the following way: $0.1\times0.1\times0.1$ mm^3 voxels for distances in the range of $r_{\text{source}}<r\leq1$ cm, $0.5\times0.5\times0.5$ mm^3 voxels for 1 cm$<r\leq5$ cm, $1\times1\times1$ mm^3 voxels for 5 cm$<r\leq10$ cm, and $2\times2\times2$ mm^3 voxels for 10 cm$<r\leq20$ cm, where r is defined as the distance from the center of the source. The magnitude of error introduced by voxel size effects is discussed by Ballester *et al.*[28] and our previous study[8] and is typically less than 0.25%.

Calculations of the air kerma per history are made *in vacuo*, thereby avoiding the need to correct for attenuation by air. The mass energy absorption coefficients for air used in this calculation are calculated with the composition recommended by TG-43U1 (40% humidity).[3] Air kerma times d^2 per history is calculated in a $10\times10\times0.05$ cm^3 voxel located 100 cm from the source along the transverse axis and then corrected to give the air kerma times d^2 per history at a point (assuming an isotropic point source) as described in our previous study.[8] In this case the correction is only 0.22% due to the large distance between the source and scoring voxel. While measurements of air kerma strength for ^{192}Ir sources are generally made at a point on the transverse axis, the large voxel is used in this case to increase the efficiency of the calculation. Reducing the voxel size to $1\times1\times0.05$ cm^3 did not change the calculated air kerma strength within statistical uncertainties. Low-energy photons emitted from the source encapsulation are suppressed in the air kerma calculations by discarding all photons with energy less than 10 keV (i.e., PCUT set to 10 keV in EGSnrc). Decreasing the photon cutoff energy to 1 keV does not change the value of the air kerma strength significantly.

II.C. TG-43 dosimetry parameters

TG-43 parameters are calculated in the same way described by our previous studies.[8,1] However, unlike ^{125}I and ^{103}Pd seeds, ^{192}Ir and ^{169}Yb sources are generally not symmetric about the transverse axis and therefore dosimetry parameters must be tabulated over a range of $0°\leq\theta\leq180°$. For all calculations in this study, r is defined as the distance from the center of the active region of the source and 0° and 180° are considered to be the distal and proximal (attached to the cable) ends of the sources, respectively. When tabulation points for the dosimetry parameters do not correspond with the center of a voxel, dose values are interpolated bi-linearly using the nearest neighbors of the voxel that the point of interest falls within. To improve the accuracy of the interpolation, all dose values are first divided by their respective values of the geometry function,[2,3] $G_L(r,\theta)$, which is associated with the voxel's geometric center.

Dose rate constants, Λ, are calculated by dividing the dose-to-water per history in a (0.1 mm)^3 voxel centered on the reference position (1 cm, 90°) in the $80\times80\times80$ cm^3 water phantom by the air kerma times d^2 per history. Similar to the studies by Medich *et al.*,[25,30] the air kerma per history in this study is calculated *in vacuo* on the transverse axis 100 cm from the source as described above. This technique differs from the extrapolation technique used in most studies of ^{192}Ir sources (see, for example, Ref. 31) where air kerma strength is scored in air along the transverse axis, fit to a linear function and then extrapolated back to zero distance to correct for the scatter and attenuation in air. In this study both techniques are found to produce equivalent results. For example, for the microSelectron v2, the dose rate constant calculated with an air kerma per history scored in a voxel at 100 cm gives $\Lambda=1.109(2)$ cGy h^{-1} U^{-1} while the extrapolation method of calculating air kerma per history gives $\Lambda=1.108(2)$ cGy h^{-1} U^{-1}. Here and throughout the rest of this paper the number in parentheses following a value represents the absolute uncertainty on the last digit of the value with an index of coverage of $k=1$.

The radial dose function, $g(r)$, is calculated using both line and point source geometry functions and tabulated at 31 distances over a range of 0.2 cm$\leq r\leq$20 cm. Radial dose functions are also fit over the range of 0.2 cm$\leq r\leq$20 cm using both the fifth order polynomial recommended by TG-43 and the modified polynomial function,

$$g(r)=(a_0r^{-2}+a_1r^{-1}+a_2+a_3r+a_4r^2+a_5r^3)e^{-a_6r}, \qquad (1)$$

introduced by our recent paper.[32] Using the normalization of the $g(r)$ data as described in our previous paper,[1] the modified polynomial fit resulted in a function which is unity at $r=1$ cm and the raw data for $g(r)$ at 1 cm is within 0.1% of unity. Fits using the modified polynomial have maximum and average residuals (as defined in Ref. 32) of less than 0.62% and 0.13%, respectively, for all sources. Fifth order polynomial fits are also found to be sufficient for fitting the radial dose function data over the same range of distances with maximum and average residuals less than 2.8% and 0.25%, respectively, for all sources. Fitting parameters for both types of functions are provided on the CLRP web site.

Anisotropy functions, $F(r,\theta)$, are calculated using the line source approximation for all sources and tabulated at radii of 0.25, 0.5, 0.75, 1, 2, 3, 4, 5, 7.5, 10, 12.5, 15, and 20 cm and 47 polar angles with a maximum difference of 5°. For $\theta\leq10°$ the anisotropy function is tabulated at θ=0°, 1°, 2°, 3°, 5°, 7°, and 10° (and the corresponding angles at the distal end of the source). The anisotropy factor, $\phi_{an}(r)$, is calculated by integrating the solid-angle-weighted dose rate over $0°\leq\theta\leq180°$ excluding points that fall within the source encapsulation or attached wire.

Dose distributions surrounding the sources are also tabulated in "along-away" tables with doses per history normalized to the air kerma times d^2 per history and tabulated on a rectangular grid. Along and away distances used in this study are at 0 cm and ±0.2, 0.4, 0.6, 0.8, 1, 1.5, 2, 3, 4, 5, 7.5, 10, 12.5, 15, and 20 cm. For these tables the "along" direction is

parallel to the source (z) axis and the "away" direction is parallel to the transverse axis. The positive and negative "along" directions are equivalent to the distal ($\theta=0°$) and proximal ($\theta=180°$) ends of the sources, respectively. Doses from opposite sides of the seed axis are averaged to partially take advantage of the simulation symmetry. When tabulation points do not correspond to the center of a voxel, doses are interpolated bi-linearly using the nearest neighbor voxels as described above. For the set of along-away tabulations points in this study, interpolation is only required when "along" or "away" is equal to 12.5 cm as the rest of the points all fall at the center of a voxel.

II.D. Calculations of primary and scatter dose separation

In addition to scoring the total dose per history, the dose is scored separately for primary, single-scattered, and multiple-scattered photons according to the PSS formalism.[9] In this study any photon escaping the source encapsulation is considered to be a primary. For example, if a photon undergoes a Compton scattering event before escaping the source encapsulation, it is still scored as a primary photon until a scattering event occurs in the phantom medium itself. Scatter dose calculations are benchmarked against similar calculations made by Carlsson and Ahnesjö[11,12] and Russell and Ahnesjö.[33]

The total, primary, single scatter, and multiple scatter separated doses are labeled as $D_{to}(r,\theta)$, $D_{pr}(r,\theta)$, $D_{ss}(r,\theta)$, and $D_{ms}(r,\theta)$, respectively. Total, primary and scatter separated doses are all normalized to the sources total radiant photon energy, R, defined as the sum of the energy of all photons escaping the source encapsulation. Normalizing the dose in this manner yields units of inverse mass (in g^{-1}) for $D_i(r,\theta)$. The (r,θ) coordinate system and the tabulation points for $D_i(r,\theta)$ are the same as described above for the TG-43 dosimetry parameters. When scatter dose tabulation points do not fall at the center of a voxel, dose values are interpolated as described in Sec. II C.

II.E. Energy-weighted photon spectra calculations

The normalized energy-weighted photon spectrum of photons exiting a source is scored as,

$$\frac{dR(E_j)}{dE} \Big/ R = \sum_i E_i \Big/ (\Delta E \cdot R), \tag{2}$$

where E_j is the energy of the middle of a bin, E_i is the energy of the ith photon escaping the encapsulation or cable with energies between $E_j \pm \Delta E/2$, and ΔE is the bin width. Energy-weighted photon spectra are normalized to the total radiant photon energy, R, as defined in Sect. II D. yielding units of MeV^{-1}. The bin width ΔE is set to 1 keV for all spectral calculations.

III. DETAILED SOURCE DESCRIPTIONS

This section gives a detailed description of each source modelled in our Monte Carlo calculations with Yegin's multi-geometry package.[16] Since there is no consensus on what is the proper amount of cable to include in MC simulations, the cable lengths in this study have been chosen, whenever possible, to be the same as previous studies. This facilitates comparison of dosimetry parameters between this study and previous studies. All 15 of the sources, drawn to the same scale, are pictured in Fig. 2 and summaries of the materials and geometry are given in Table I. The same descriptions along with to-scale drawings are on the web resource.

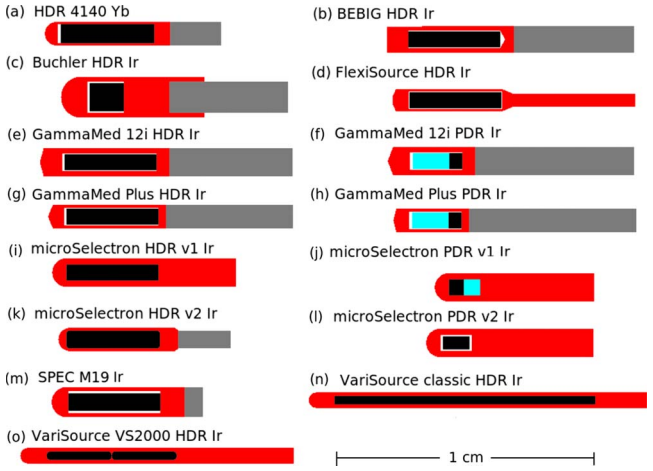

FIG. 2. Scale drawings of all the sources investigated in this study. From top-to-bottom, left-to-right the sources are (a) Implant Sciences 4140 HDR, (b) BEBIG GI192M11 HDR, (c) Buchler G0814 HDR, (d) IsoDose Flexisource, (e) GammaMed 12i HDR, (f) GammaMed 12i PDR, (g) GammaMed Plus HDR, (h) GammaMed Plus PDR, (i) microSelectron v1 (classic) HDR, (j) microSelectron v1 (classic) PDR, (k) microSelectron v2 HDR, (l) microSelectron v2 PDR, (m) SPEC M19, (n) VariSource (classic), and (o) VariSource VS2000. All sources are drawn to the same scale, are aligned along the approximate center of activity, and have their active regions colored black. Some of the simulations included more cable attached to the sources than is pictured here.

III.A. High dose rate ^{169}Yb source

III.A.1. Implant sciences, 4140, HDR

Dimensions for the HDR 4140 source [see Fig. 2(a)] are taken from the study by Medich *et al.*[25] The 4140 source consists of a 3.60 mm long cylindrical ytterbium oxide core (6.9 g/cm^3) with a diameter of 0.73 mm that is enclosed in a stainless steel capsule (assumed to be AISI 306 with a density of 7.80 g/cm^3). The encapsulation includes a 0.50 mm thick end weld composed of a 0.45 mm radius hemisphere attached to a 0.050 mm thick solid cylinder. The end weld is attached to a 4.30 mm long hollow cylindrical section that has inside and outside diameters of 0.73 and 0.90 mm, respectively. The hollow portion of the encapsulation is attached to a solid cylindrical section that is 0.60 mm thick and 0.90 mm in diameter. The empty space between the encapsulation and the source element is assumed to be filled with air. The cable is assumed to be a solid cylinder of AISI 306 stainless steel with an effective density of 6.90 g/cm^3, a diameter of 0.90 mm, and a length of 1.95 mm. The active length of the source is 3.6 mm.

TABLE I. Summary of the source materials and geometries used in this study. All of the sources except the last have ^{192}Ir cores with a density of 22.42 g/cm^3 and the HDR 4140 has an Yb_2O_3 core with a density of 6.90 g/cm^3. AISI are different types of steel.

		Active core		Encapsulation		
Seed Name	Type	L (mm)	O.D. (mm)	Material	Thickness (mm)	O.D (mm)
Buchler G0814 (Ref. 35)	HDR ^{192}Ir	1.3	1.00	AISI 321	0.200	1.60
BEBIG G1192M11 (Ref. 34)	HDR ^{192}Ir	3.5	0.60	AISI 316L	0.150	1.00
GammaMed 12i (Ref. 38)	HDR ^{192}Ir	3.5	0.70	AISI 316L	0.200	1.10
GammaMed 12i (Ref. 40)	PDR ^{192}Ir	0.5	0.60	AISI 316L	0.200	1.10
GammaMed Plus (Ref. 38)	HDR ^{192}Ir	3.5	0.70	AISI 316L	0.100	0.90
GammaMed Plus (Ref. 40)	PDR ^{192}Ir	3.5	0.70	AISI 316L	0.100	0.90
IsoDose Control Flexisource (Ref. 37)	HDR ^{192}Ir	3.5	0.60	AISI 304	0.090	0.85
Nucletron microSelectron v1 (Refs. 31 and 41)	HDR ^{192}Ir	3.5	0.60	AISI 304	0.250	1.10
Nucletron microSelectron v1 (Refs. 31 and 44)	PDR ^{192}Ir	0.6	0.60	AISI 316L	0.250	1.10
Nucletron microSelectron v2 (Refs. 45 and 18)	HDR ^{192}Ir	3.6	0.65	AISI 316L	0.125	0.90
Nucletron microSelctron v2 (Ref. 44)	PDR ^{192}Ir	1.0	0.50	AISI 316L	0.250	1.10
SPEC M19 (Ref. 30)	HDR ^{192}Ir	3.5	0.65	AISI 306	0.160	1.10
Varian VariSource classic (Refs. 47, 49, 48, and 18)	HDR ^{192}Ir	10.0	0.34	Ni/Ti	0.125	0.59
Varian VariSource VS2000 (Ref. 50)	HDR ^{192}Ir	5.0	0.34	Ni/Ti	0.125	0.59
Implant Sciences 4140 (Ref. 25)	HDR ^{169}Yb	3.6	0.73	AISI 306	0.085	0.90

III.B. Pulsed and high dose rate ^{192}Ir sources

III.B.1. BEBIG, GI192M11, HDR

Dimensions for the BEBIG GI192M11 source [see Fig. 2(b)] are taken from the study by Granero *et al.*[34] The BEBIG source consists of a 3.50 mm long cylindrical Ir core with a diameter of 0.60 mm enclosed in a 1.00 mm diameter AISI 316L stainless steel capsule (density of 7.8 g/cm^3). The encapsulation is a 0.84 mm long solid cylindrical section followed by a 3.50 mm long hollow section with an inner diameter assumed to be 0.70 mm. The last section of the capsule is a 0.55 mm long solid cylinder overlapped by an air cone with a height of 0.20 mm and an opening angle of 60°. A total of 6 cm of cable is included in this simulation and the cable is assumed to be composed of AISI 316L steel with an effective density of 6.9 g/cm^3. The active length of this source is 3.50 mm.

III.B.2. Buchler, G0814, HDR

Dimensions for the Amersham Buchler source[35,36] [see Fig. 2(c)] are taken from the study by Ballester *et al.*[35] The Buchler source consists of a 1.30 mm long Ir core with a diameter of 1.00 mm enclosed in an AISI 321 stainless steel capsule with a density of 8.027 g/cm^3. The end of the encapsulation is a 1.60 mm diameter hemisphere offset from the center of the source by 0.95 mm. The cavity containing the Ir source is a 1.40 mm long cylindrical shell with inner and outer diameters of 1.20 and 1.60 mm, respectively. Next to the cavity there is a 1.76 mm long solid cylindrical section with a diameter of 1.60 mm followed by a 1.34 mm long cylindrical shell with inner and outer diameters of 1.10 and 1.60 mm, respectively. Inserted into this hollow section is a 6 cm long section of AISI 301 stainless steel cable (effective density of 8.00 g/cm^3) with an outer diameter of 1.10 mm. The active length of this source is 1.30 mm.

III.B.3. IsoDose control, Flexisource, HDR

Dimensions for the Flexisource [see Fig. 2(d)] are taken from the study by Granero *et al.*[37] The Flexisource consists of a 3.50 mm long Ir core with a diameter of 0.60 mm enclosed in a 0.85 mm diameter AISI 304 stainless steel capsule (density of 8.02 g/cm^3). The tip of the encapsulation is assumed to be a 0.108 mm thick conical section with a half angle of 23.6° and the radius of the face being 0.17 mm. The conical section is attached to a 0.49 mm long solid cylindrical section followed by a 3.6 mm long hollow section with an inner diameter of 0.67 mm. Following the hollow section is a 0.40 mm long solid conical section with a half-angle assumed to be 24°. Attached to the conical section is a 5 mm long section of AISI 304 stainless steel cable. The active length of this source is 3.50 mm.

III.B.4. GammaMed, 12i, HDR

Dimensions for the GammaMed 12i HDR source[38,39,36] [see Fig. 2(e)] are taken from the study by Ballester *et al.*[38] The 12i source consists of a 3.50 mm long Ir core with a diameter of 0.70 mm enclosed in a 1.10 mm diameter AISI 316L stainless steel capsule (density of 7.8 g/cm^3). The tip of the encapsulation is a conical section with a height of 0.143 mm and a half-angle of 75°. The cone is attached to a 0.717 mm long solid cylindrical section followed by a 3.60 mm long hollow section with an inner diameter assumed to be 0.70 mm. Following the hollow section is a 0.50 mm long solid cylindrical section. A total of 6.00 cm of AISI 304 stainless steel cable (effective density of 5.6 g/cm^3) is included in this simulation. The active length of this source is 3.50 mm.

III.B.5. GammaMed, 12i, PDR

Dimensions of the GammaMed 12i PDR source [see Fig. 2(f)] are taken from the study by Perez-Calatayud *et al.*[40] The 12i source consists of a 0.50 mm long Ir core with a diameter of 0.60 mm enclosed in a 1.10 mm diameter AISI 316L stainless steel capsule (density of 7.8 g/cm^3). Next to the Ir core (distal end of the source) is a 1.4 mm long solid cylinder of Al with a diameter of 0.60 mm. The tip of the encapsulation is a conical section with a height of 0.20 mm and an opening angle of 70°. The cone is attached to a 0.66 mm long solid cylindrical section followed by a 2.00 mm long hollow section with an inner diameter of 0.70 mm. Following the hollow section is a 0.50 mm long solid cylindrical section. A total of 6.0 cm of AISI 304 stainless steel cable (effective density of 5.6 g/cm^3) is included in this simulation. The active length of this source is 0.50 mm.

III.B.6. GammaMed, Plus, HDR

Dimensions for the GammaMed Plus HDR source[38,39,36] [see Fig. 2(g)] are taken from the study by Ballester *et al.*[38] The Plus source consists of a 3.50 mm long Ir core with a diameter of 0.70 mm enclosed in a 0.90 mm diameter AISI 316L stainless steel capsule (density of 7.8 g/cm^3). The tip of the encapsulation is a conical section with a height of 0.183 mm and an opening angle of 68°. The cone is attached to a 0.50 mm long solid cylindrical section followed by a 3.60 mm long hollow section with an inner diameter assumed to be 0.70 mm. Following the hollow section is a 0.30 mm long solid cylindrical section. A total of 6.00 cm of AISI 304 stainless steel cable (effective density of 5.6 g/cm^3) is included in this simulation. The active length of this source is 3.50 mm.

III.B.7. GammaMed, Plus, PDR

Dimensions for the GammaMed Plus PDR source [see Fig. 2(h)] are taken from the study by Perez-Calatayud *et al.*[40] The Plus source consists of a 0.50 mm long Ir core with a diameter of 0.60 mm enclosed in a 0.90 mm diameter AISI 316L stainless steel capsule (density of 7.8 g/cm^3). Next to the Ir core (distal end of the source) is a 1.4 mm long solid cylinder of Al with a diameter of 0.60 mm. The tip of the encapsulation is a conical section with a height of 0.12 mm and an opening angle of 75°. The cone is attached to a 0.50 mm long solid cylindrical section followed by a 2.00 mm long hollow section with an inner diameter of 0.70 mm. Following the hollow section is a 0.30 mm long solid cylindrical section. A total of 6.0 cm of AISI 304 stainless steel cable (effective density of 5.6 g/cm^3) is included in this simulation. The active length of this source is 0.50 mm.

III.B.8. Nucletron, microSelectron v1 (classic), HDR

Dimensions for the microSelectron v1 HDR[31,41–43] [see Fig. 2(i)] are taken from the study by Williamson and Li.[31] The microSelectron consists of a 3.50 mm long Ir core with 0.60 mm diameter contained in an AISI 304 stainless steel wire with a diameter of 1.10 mm (should have been AISI 316L, however the differences are negligible). The end of the wire is modelled as a 0.55 mm diameter hemisphere with its center shifted 0.1755 mm from the center of the source. A length of cable extending 4.75 mm from the center of the source is included in this simulation. The active length of this source is 3.50 mm.

III.B.9. Nucletron, microSelectron v1 (classic), PDR

Dimensions for the microSelectron v1 PDR source[31,44] [See Fig. 2(j)] are taken from the study by Karaiskos *et al.*[44] The source consists of two 0.60 mm long Ir cores with a diameter of 0.60 mm enclosed in an AISI 316L stainless steel capsule (with a density of 8.06 g/cm^3). Only the distal Ir core is radioactive and the origin for this source is thus placed at the center of the distal core. The encapsulation consists of a 0.55 mm thick hemispherical end weld. The end weld is attached to a 1.20 mm long hollow cylindrical section that has inside and outside diameters of 0.60 and 1.10 mm, respectively. The remainder of the encapsulation and cable is modelled as a solid cylinder with a radius of 1.1 mm and a length of 4.65 mm. The cable is also assumed to be AISI 316L stainless steel. The active length of the source is 0.60 mm.

III.B.10. Nucletron, microSelectron v2, HDR

Dimensions for the microSelectron v2 HDR[45,46,42,43] [see Fig. 2(k)] are taken from the study by Daskalov *et al.*[45] The microSelectron consists of a 3.60 mm long Ir core with a diameter of 0.65 mm enclosed in a 0.90 mm diameter AISI 316L stainless steel capsule (density 8.06 g/cm^3). The Ir core is modelled as a 3.48 mm long cylindrical section attached to two 0.265 mm long conical sections (45°) to approximate the rounded ends of the real source. The tip of the encapsulation is modelled as a 0.45 mm hemisphere with its center shifted 1.65 mm from the center of the source. The end of the encapsulation attached to the cable is modelled as a 0.15 mm thick conical section (half angle of 33.7°) starting 1.20 mm from the center of the source. Attached to the conical section is a 2.00 mm long section of AISI 316L stainless steel cable with an effective density of 4.81 g/cm^3. The active length of this source is 3.60 mm.

III.B.11. Nucletron, microSelectron v2, PDR

Dimensions for the microSelectron v2 PDR source [see Fig. 2(l)] are taken from the study by Karaiskos *et al.*[44] The source consists of two 0.50 mm long Ir cores with a diameter of 0.50 mm (modelled in this study as a 1.0 mm long solid cylinder) enclosed in an AISI 316L stainless steel capsule (with a density of 8.06 g/cm^3). The encapsulation consists of a 0.50 mm thick end weld composed of a 0.55 mm radius hemisphere overlapped with a 0.05 mm thick solid cylinder of air. The end weld is attached to a 1.20 mm long hollow cylindrical section that has inside and outside diameters of 0.60 and 1.10 mm, respectively. The remainder of the encapsulation and cable is modelled as a solid cylinder with a radius of 1.1 mm and a length of 4.65 mm. The cable is also

assumed to be AISI 316L stainless steel. All empty space is filled with air. The active length of the source is 1.0 mm.

III.B.12. SPEC, M19, HDR

Dimensions for the M19 source [see Fig. 2(m)] are taken from the study by Medich and Munro.[30] The M19 source consists of a 3.50 mm long cylindrical Ir core with a diameter of 0.65 mm enclosed in a stainless steel capsule (assumed to be AISI 306 with a density of 7.80 g/cm^3). The encapsulation consists of an end weld composed of a 0.65 mm thick section of a hemisphere that is 1.17 mm in diameter attached to a 3.50 mm long hollow cylindrical section with inside and outside diameters of 0.85 and 1.17 mm, respectively. The hollow portion of the encapsulation is attached to a solid cylindrical section that is 0.950 mm thick and 1.17 mm in diameter. The cable is assumed to be a solid cylinder of AISI 306 stainless steel with an effective density of 6.90 g/cm^3, a diameter of 1.17 mm, and a length of 0.71 mm.

III.B.13. Varian, VariSource classic, HDR

Dimensions for the VariSource classic[47–49,18,50,42,43] [see Fig. 2(n)] are taken from the study by Karaiskos *et al.*[48] The VariSource consists of a 10.0 mm long Ir core with 0.34 mm diameter contained in a 55.6%/44.4%-Ni/Ti wire with a diameter of 0.59 mm. The end of the wire is modelled as a hemisphere with its center shifted 0.5705 mm from the center of the source. A length of wire extending 5.00 cm from the center of the source is included in this simulation. The active length of this source is 10.0 mm.

III.B.14. Varian, VariSource VS2000, HDR

Dimensions for the VariSource VS2000 [see Fig. 2(o)] are taken from the study by Angelopoulos *et al.*[50] The VS2000 consists of two 2.50 mm long Ir cores. Each source is made up of a 2.16 mm long cylindrical section with a 0.34 mm diameter and hemispherical ends with the same diameter. The two sources are contained in a 55.6%/44.4%-Ni/Ti wire with a diameter of 0.59 mm. The end of the wire is modelled as a hemisphere with its center shifted 3.205 mm from the center of the source. A length of wire extending 5.00 cm from the center of the source is included in this simulation. The active length of this source is 5.00 mm.

IV. RESULTS AND DISCUSSION

Due to the large amount of data generated during this study, only the dose rate constants calculated in this study and by other authors are presented here. The entire dosimetry dataset, including TG-43 dosimetry parameters, along-away dose tables, energy-weighted photon spectra, and scatter/primary dose tables, is available at http://www.physics.carleton.ca/clrp/seed_database/. Also included on the website are fits to the radial dose functions for 0.2 cm$\leq r \leq$20 cm using fifth order polynomials and the functional form given in Eq. (1). Calculated dose rate constants and their statistical uncertainties from this study and studies by other authors are listed in Table II.

Uncertainties reported on dosimetry values calculated in this study are statistical uncertainties only. Statistical uncertainties on dose rate constants calculated in this study are generally less than 0.3%, while radial dose function and anisotropy function values have statistical uncertainties of less than 0.5% at distances up to 20 cm from the center of the source. Multiple scatter, single scatter, and primary dose data have statistical uncertainties of less than 0.5% and 1% at r=10 cm and r=20 cm, respectively. Other sources of uncertainty in these calculations include uncertainties in cross section data, source geometry, and material definitions and the effects of ignoring electron transport. Scoring dose in voxels also introduces some uncertainty as discussed in Ref. 8. Due to the large number of factors affecting the uncertainty of these calculations, a separate study would be required to derive a meaningful estimate of the overall uncertainty. However, the combined uncertainties from the sources listed above are greater than the statistical uncertainties on dosimetry parameters calculated in this study.

IV.A. TG-43 dosimetry parameters

TG-43 dosimetry parameters calculated in this study are in excellent agreement with values calculated previously by other authors. Dose rate constants from this study agree with values calculated by other authors within statistical uncertainties for all sources.

Radial dose functions from this study are also generally in excellent agreement (less than 1% difference over 0.2 cm$\leq r \leq$20 cm) with values calculated in studies by other authors who use an effectively infinite scattering medium. Previous studies of five sources (microSelectron v1 HDR,[31,41] microSelectron v1 PDR,[31,41] microSelectron v2 HDR,[45] VariSource classic[47,48] and VariSource VS2000[50]) used a 30 cm diameter spherical water phantom, which does not provide a full scattering medium.[27] For these five sources, radial dose function values calculated at 10 and 15 cm are roughly 7% and 35% higher in this study than values calculated previously by other authors. In addition to calculations using a full scattering medium, a full set of calculations is performed for the microSelectron v2 source in a 30 cm diameter water phantom. For this set of calculations the radial dose functions for the microSelectron v2 source agree within 1% of the values calculated by Daskalov *et al.*[45] A comparison of the radial dose functions for both phantom sizes is presented in Fig. 3(a).

Anisotropy function data in this study are generally in very good agreement with values from other studies (usually less than a 2% difference). There are a few notable differences between anisotropy data calculated in this study and data calculated by other authors. The differences all occur for values of $r \leq 1$ cm and for small values of θ close to the seed axis, where dose gradients are steepest. Anisotropy function data calculated in this study for the ^{169}Yb HDR 4140 source are as much as 10% higher than the values calculated by Medich *et al.*[25] for $\theta \leq 10°$ and $r \leq 1$ cm. For $\theta \geq 20°$ the differences are less than 3%. For the Buchler GO814 source,

TABLE II. Dose rate constants and uncertainties calculated in this study and by other authors for ^{192}Ir and ^{169}Yb sources. In two cases dose rate constants for a reference depth of r_o=0.2 cm are given for comparison to previous results.

Manufacturer & seed name	Type	Author	Method	Λ cGy h^{-1} U^{-1}
Buchler G0814	HDR ^{192}Ir	This study	voxel at 100 cm	1.119±0.003
		Ballester *et al.* (Ref. 35)	extrapolated	1.115±0.003
BEBIG GI M11	HDR ^{192}Ir	This study	voxel at 100 cm	1.112±0.002
		Granero *et al.* (Ref. 34)	extrapolated	1.108±0.003
GammaMed 12i	HDR ^{192}Ir	This study	voxel at 100 cm	1.117±0.002
		Ballester *et al.* (Ref. 38)	extrapolated	1.118±0.003
GammaMed 12i	PDR ^{192}Ir	This study	voxel at 100 cm	1.127±0.003
		Perez-Calatayud *et al.* (Ref. 40)	extrapolated	1.122±0.003
GammaMed Plus	HDR ^{192}Ir	This study	voxel at 100 cm	1.115±0.002
		Ballester *et al.* (Ref. 38)	extrapolated	1.118±0.003
GammaMed Plus	PDR ^{192}Ir	This study	voxel at 100 cm	1.125±0.003
		Perez-Calatayud *et al.* (Ref. 40)	extrapolated	1.122±0.003
IsoDose Control Flexisource	HDR ^{192}Ir	This study	voxel at 100 cm	1.116±0.003
		Granero *et al.* (Ref. 37)	extrapolated	1.109±0.011
Nucletron microSelectron v1 (classic)	HDR ^{192}Ir	This study	voxel at 100 cm	1.117±0.002
		Williamson and Li (Ref. 31)	extrapolated	1.115±0.006
		Karaiskos *et al.* (Ref. 41)	extrapolated	1.116±0.006
Nucletron microSelectron v1 (classic)	PDR ^{192}Ir	This study	voxel at 100 cm	1.126±0.002
		Williamson and Li (Ref. 31)	extrapolated	1.128±0.006
		Karaiskos *et al.* (Ref. 44)	extrapolated	1.124±0.006
Nucletron microSelectron v2	HDR ^{192}Ir	This study	voxel at 100 cm	1.109±0.002
		this study	r_o=0.2 cm/voxel at 100 cm	22.73±0.02
		Daskalov *et al.* (Ref. 45)	extrapolated	1.108±0.001
		Wang and Li (Ref. 18)	r_o=0.2 cm/voxel at 100 cm	22.75±0.03
Nucletron microSelectron v2	PDR ^{192}Ir	this study	voxel at 100 cm	1.119±0.002
		Karaiskos *et al.* (Ref. 44)	extrapolated	1.121±0.006
SPEC M19	HDR ^{192}Ir	this study	voxel at 100 cm	1.114±0.002
		Medich and Munro (Ref. 30)	voxel at 100 cm	1.13±0.03
Varian VariSource Classic	HDR ^{192}Ir	this study	voxel at 100 cm	1.042±0.002
		this study	r_o=0.2 cm/voxel at 100 cm	13.00±0.02
		Wang and Sloboda (Ref. 47)	extrapolated	1.044±0.002
		Karaiskos *et al.* (Ref. 48)	voxel at 15 cm	1.043±0.005
		Meigooni *et al.* (Ref. 49)	TLD	1.084±0.043
		Meigooni *et al.* (Ref. 49)	radiochromic film	1.054±0.053
		Wang and Li (Ref. 18)	r_o=0.2 cm/extrapolated	13.12±0.03
Varian VariSource (VS2000)	HDR ^{192}Ir	this study	voxel at 100 cm	1.099±0.002
		Angelopoulos *et al.* (Ref. 50)	extrapolated	1.101±0.006
Implant Sciences 4140	HDR ^{169}Yb	this study	voxel at 100 cm	1.186±0.003
		Medich *et al.* (Ref. 25)	voxel at 100 cm	1.19±0.03

anisotropy function values calculated in this study are up to 4% higher than the values calculated by Ballester *et al.*[35] for $\theta \leq 10°$ and $r \leq 1$ cm. At θ=15° this difference drops to 0.5%. Anisotropy data for the microSelectron v2 source calculated in this study are roughly 5% higher than the values calculated by Daskalov *et al.*[45] for r=0.25 cm and $\theta \leq 10°$.

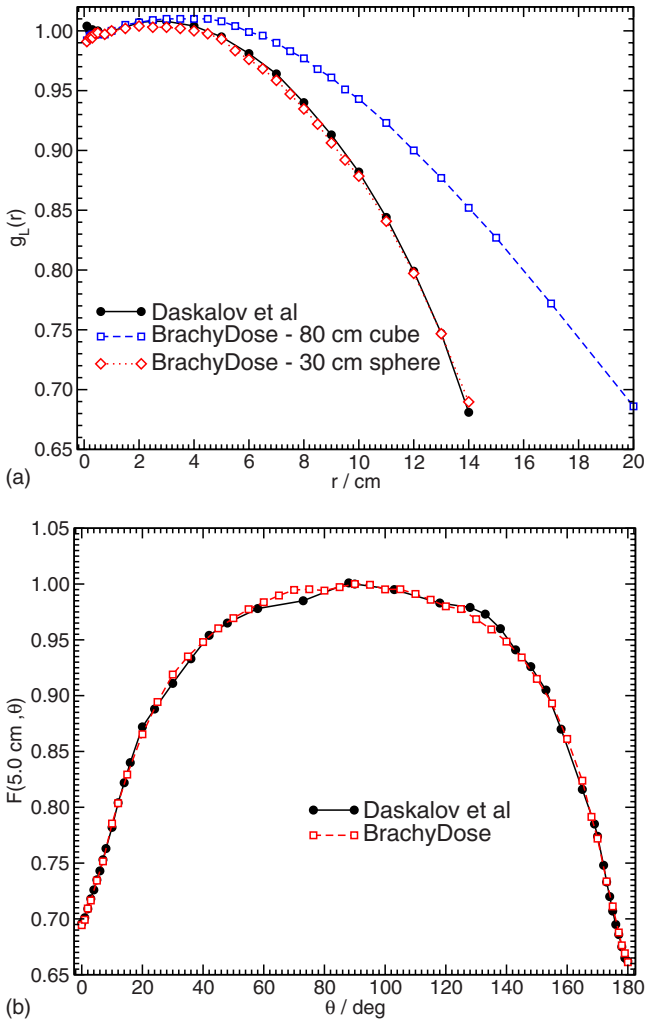

FIG. 3. Radial dose function data, $g_L(r)$, for the microSelectron v2 source calculated in a cubic $(80\ \text{cm})^3$ phantom and a 30 cm diameter spherical phantom are shown in (a). Radial dose functions calculated in the cubic phantom are roughly 7% and 35% higher than in the spherical phantom at 10 and 15 cm, respectively. Anisotropy function values calculated in the $(80\ \text{cm})^3$ phantom at $r=5.0$ cm are shown in (b). Data from Daskalov *et al.* (Ref. 45) calculated in a 30 cm diameter spherical phantom, are also included for comparison in both figures.

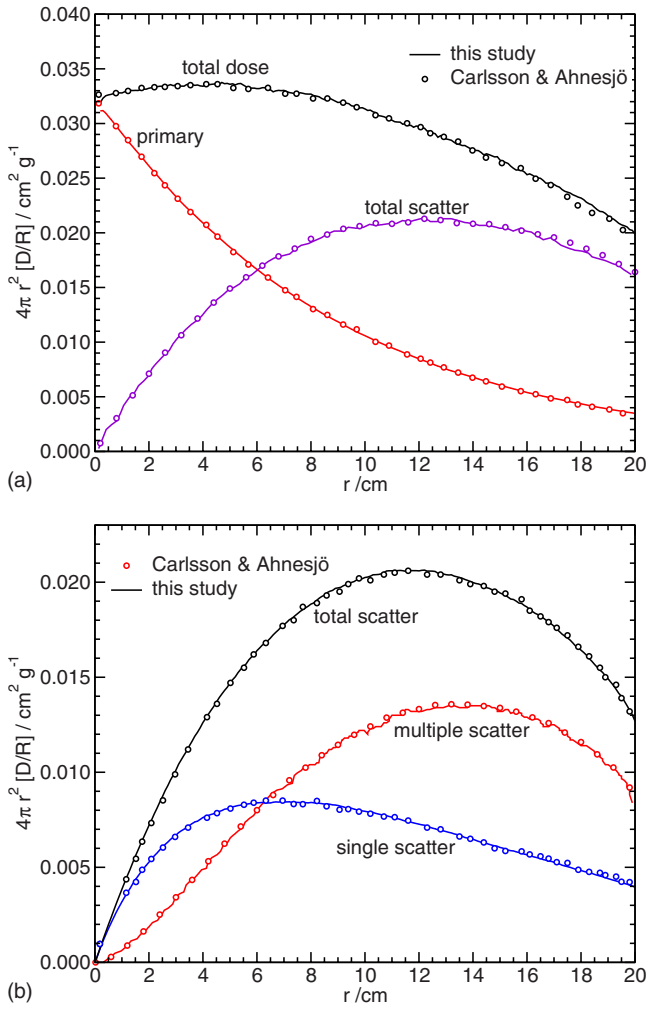

FIG. 4. Primary and scattered dose times $4\cdot\pi\cdot r^2$ for a 350 keV point source of photons in a water phantom, scored in 0.1 cm thick concentric spherical shells. (a) is for a $20\times20\times20$ cm^3 water phantom (Ref. 11) while (b) uses a 40 cm diameter spherical phantom (Ref. 12). Lines are doses calculated in this study while symbols are doses calculated by Carlsson and Ahnesjö (Refs. 11 and 12). All data are normalized independently to give the dose times $4\cdot\pi\cdot r^2$ per radiant photon energy (R).

For the microSelectron v2 source, these differences do not appear to be due to voxel size issues as dose calculated with a voxel size of $(0.05\ \text{mm})^3$ did not differ from that calculated using the $(0.1\ \text{mm})^3$ voxel at $r=0.25$ cm. If the differences were due to photon cross sections, one would expect similar differences to be seen at $r=0.5$ cm, however, both sets of data are in agreement within 1% here. While the explanation of these differences is currently unresolved, it may be somewhat of a moot issue since the differences mostly occur within 0.2 cm of the source encapsulation. As discussed above in Sec. II B. this study is not reporting dosimetry parameters within 0.2 cm of the source encapsulation as there may be significant differences between the dose and kerma in this region and the dose from the beta spectrum of ^{192}Ir is not accounted for by any of the studies discussed in this section.

For the microSelectron v2 source, anisotropy values calculated for the 30 cm diameter spherical phantom are compared with values calculated for the $80\times80\times80$ cm^3 cubic phantom. It is found that phantom size has little effect on the anisotropy function as the two sets of calculations are in agreement within 2% at $r=10$ cm and 0.5% for $r\leq5$ cm. Anisotropy function data at $r=5.0$ cm calculated in this study and the study by Daskalov *et al.*[45] are compared in Fig. 3(b).

IV.B. Primary and scatter dose separation data

Figure 4(a) shows comparisons of total dose, scatter dose and primary dose calculated in this study and by Carlsson and Ahnesjö.[11] These calculations are made for a 350 keV mono-energetic point source of photons (approximately the average energy of the ^{192}Ir spectrum) located at the center of a $20\times20\times20$ cm^3 water phantom. In this study, dose is scored in concentric spherical shells 1 mm thick. Data from

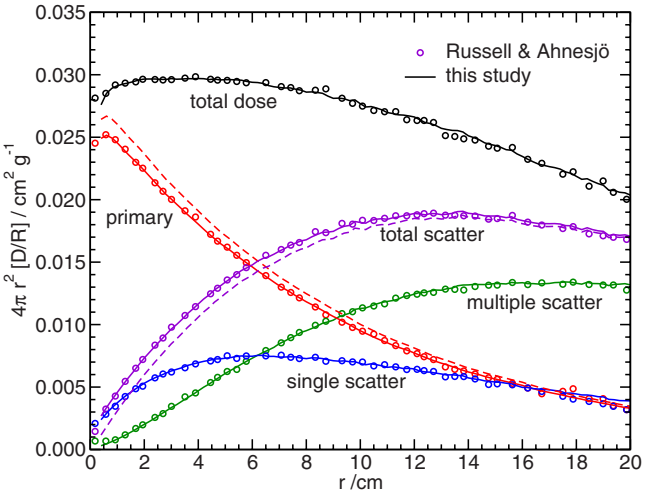

FIG. 5. Primary and scattered dose $\times 4\pi r^2$ data along the transverse axis of the 0.35 mm long ^{192}Ir HDR source and nylon catheter combination described by Russell and Ahnesjö (Ref. 33). Values calculated in this study (lines) are compared with values calculated by Russel and Ahnesjö (symbols). Scoring for the calculations in this figure is slightly different than the other calculations presented in this study. In this figure dose is normalized to the total initial photon energy and photons from all scattering events (including events occurring within the source) are considered a part of the scattered dose. Dashed lines in the figure show primary and total scattered dose $\times 4\pi r^2$ scored when only scattering events occurring in the catheter and phantom are considered in the tabulation of scatter dose.

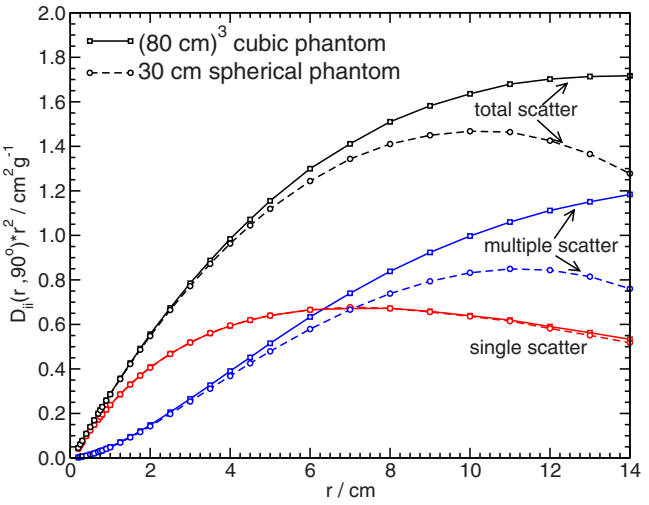

FIG. 6. The dependence of scattered dose on phantom size for the microSelectron v2 source. Single and multiple scattered dose (with the $1/r^2$ dependence removed) are compared for an $(80\ \text{cm})^3$ phantom and a spherical phantom, 30 cm in diameter. When compared with the effectively unbounded phantom, the total scatter dose in the smaller spherical phantom is reduced by 11% and 34% at 10 cm and 14 cm, respectively.

both studies are normalized independently to the total radiant photon energy, R. Our results are in excellent agreement with those of Carlsson and Ahnesjö over the entire calculated range. Figure 4(b) further separates the scattered dose into contributions from single-scattered and higher order-scattered photons. For this set of calculations dose is scored in a 40 cm diameter water sphere and compared with results from a second study by Carlsson and Ahnesjö.[12] Again there is excellent agreement between Carlsson and Ahnesjö's results and ours.

Benchmark scatter dose calculations are also done for the source and nylon catheter combination described by Russell and Ahnesjö.[33] Full details about the source and catheter can be found in their study but, briefly, the source is a 0.35 mm long ^{192}Ir core surrounded by AISI 316 stainless steel located in the middle of an air filled nylon catheter. Figure 5 shows the total, primary, and scattered dose along the transverse axis calculated in this study (lines) and the study by Russel and Ahnesjö (symbols). The phantom is a water cylinder that is 80 cm high and 80 cm in diameter and dose is scored in voxels that are 0.2 cm wide, 0.2 cm thick in the radial direction, and centered on the transverse axis. For comparison with the data of Russell and Ahnesjö, dose for these calculations is scored differently than the other calculations presented in the current study. In Fig. 5 for the solid lines, dose $\times 4\pi r^2$ is normalized to the total initial photon energy and photons from all scattering events, including events occurring within the source, are considered a part of the scattered dose tabulation. Dashed lines in the figure show primary and total scattered dose $\times 4\pi r^2$ scored when only scattering events occurring in the catheter and phantom (as opposed to the source) are considered in the tabulation of scatter dose. Only considering scattering events occurring outside the source results in total scatter (primary) dose at 1 cm that is roughly 30% lower (6% higher) than the total scatter dose when compared with tabulations considering all scattering events. At 20 cm this difference drops to less than 1% (5%) as the fluence of photons which are scattered in the source has been greatly reduced due to attenuation and most of the scattered dose is coming from photons scattered by the surrounding medium. Note that the total dose for both methods of scoring remains the same because the two methods only differ in their definition of primary vs. scatter photons.

Using the primary dose for source characterization, as in the PSS, one gets a phantom size independent quantity with only the scattered dose depending on phantom size. The dependence of scattered dose on phantom size is illustrated in Fig. 6. This figure plots $D_i(r,90°)\times r^2$ for the ^{192}Ir microSelectron v2 source, calculated both in an $(80\ \text{cm})^3$ phantom as well as a spherical phantom 30 cm in diameter. At $r=5$ cm (10 cm from the edge of the spherical phantom) there is roughly 3% more dose from multiple-scattered photons in the effectively unbounded phantom than there is in the smaller spherical phantom. This difference increases to 20% and 55% at 10 and 14 cm, respectively. Single-scattered dose is approximately equal out to $r=10$ cm but beyond 10 cm there is a slight increase in single-scattered dose in the unbounded phantom (approximately 3% at $r=14$ cm) relative to the spherical phantom. Overall the total scatter dose in the unbounded phantom is increased by 11% and 34% at 10 and 14 cm, respectively. This is consistent with our earlier findings that the radial dose function at 10 cm, $g(10\ \text{cm})$, in the unbounded phantom is 7% higher than in the spherical phantom because scattered dose makes up approximately 64% of the total dose at 10 cm $(0.64\times 0.11\simeq 0.07)$. For both phantoms, single-scattered photon dose dominates multiple-

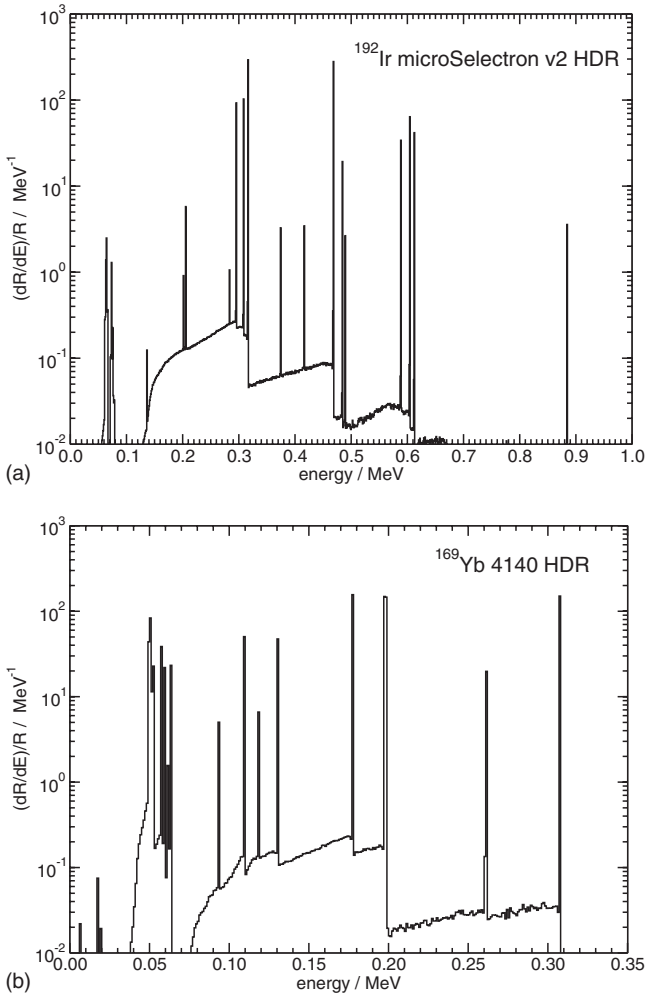

FIG. 7. Energy-weighted photon spectra per unit emitted radiant energy of photons escaping the encapsulation and cable for the (a) ^{192}Ir microSelectron v2 HDR source and (b) the ^{169}Yb HDR 4140 source. Energy-weighted photon spectra are normalized to the total radiant photon energy, R, as defined in Sec. II D yielding units of MeV^{-1}. The bin width ΔE is 1 keV.

scattered photon dose until ~6 cm from the source, at which point multiple-scattered photons make up the majority of the total scattered photon dose.

IV.C. Energy-weighted photon spectra

Figure 7 shows two examples of calculated energy-weighted photon spectra from this study. Figure 7(a) is the spectrum from the ^{192}Ir microSelectron v2 HDR source and Fig. 7(b) the spectrum emitted by the ^{169}Yb 4140 HDR source. An energy-weighted photon spectra scored in a small voxel at 100 cm distance from the center of the source on the transverse axis was also calculated for the microSelectron v2 source. The shape of the spectrum for this calculation is very similar to the spectrum including all emitted photons. All energy-weighted photon spectra calculated in this study are available on the CLRP website in graphical form as well as tabulated in "comma separated value" (.csv) text files.

V. CONCLUSION

In this study the Monte Carlo code BrachyDose is used to calculate energy-weighted photon spectra, TG-43 dosimetry parameters, and scatter dose functions for 15 high dose rate ^{192}Ir and ^{169}Yb brachytherapy sources using state-of-the art XCOM photon cross sections. TG-43 parameters are tabulated over a greater spatial extent with higher resolution than is currently available for most of the sources. This study is unique in that it provides separate tabulations of primary, single-scattered, and multiple-scattered dose data. This separation is useful for calculating the dose surrounding brachytherapy sources using convolution/superposition methods.[10–12,14,15] The complete set of dosimetry data calculated in this study is available via the Carleton Laboratory for Radiotherapy Physics website accessible at http://www.physics.carleton.ca/clrp/seed_database/. This work extends our previous work on TG-43 dosimetry parameter calculations for ^{125}I and ^{103}Pd brachytherapy seeds and makes the CLRP brachytherapy database a more complete resource.

ACKNOWLEDGEMENTS

The authors would like to thank Anders Ahnesjö of Nucletron for his useful discussions of this manuscript. The authors would also like to thank Gultekin Yegin at Celal Bayar University in Turkey for his ongoing collaboration on the development of the BrachyDose code. This work is partially funded by the Canada Foundation for Innovation, the Ontario Innovation Trust, NSERC, The Canada Research Chairs program, and Nucletron.

[a]rtaylor@physics.carleton.ca
[b]drogers@physics.carleton.ca; WWW: http://www.physics.carleton.ca/~drogers/

[1]R. E. P. Taylor and D. W. O. Rogers, "An EGSnrc Monte Carlo-calculated database of TG-43 parameters," Med. Phys. **35**, 4228–4241 (2008).
[2]R. Nath, L. L. Anderson, G. Luxton, K. A. Weaver, J. F. Williamson, and A. S. Meigooni, "Dosimetry of interstitial brachytherapy sources: Recommendations of the AAPM Radiation Therapy Committee Task Group No. 43," Med. Phys. **22**, 209–234 (1995).
[3]M. J. Rivard, B. M. Coursey, L. A. DeWerd, M. S. Huq, G. S. Ibbott, M. G. Mitch, R. Nath, and J. F. Williamson, "Update of AAPM Task Group No. 43 Report: A revised AAPM protocol for brachytherapy dose calculations," Med. Phys. **31**, 633–674 (2004).
[4]M. J. Rivard, W. M. Butler, L. A. DeWerd, M. S. Huq, G. S. Ibbott, A. S. Meigooni, C. S. Melhus, M. G. Mitch, R. Nath, and J. F. Williamson, "Supplement to the 2004 update of the AAPM Task Group No. 43 Report," Med. Phys. **34**, 2187–2205 (2007).
[5]I. Kawrakow, "Accurate condensed history Monte Carlo simulation of electron transport. I. EGSnrc, the new EGS4 version," Med. Phys. **27**, 485–498 (2000).
[6]I. Kawrakow and D. W. O. Rogers, "The EGSnrc Code System: Monte Carlo simulation of electron and photon transport," Technical Report PIRS–701, National Research Council of Canada, Ottawa, Canada, 2000.
[7]G. Yegin and D. W. O. Rogers, "A fast Monte Carlo code for multi-seed brachytherapy treatments including interseed effects," Med. Phys. **31**, 1771 (abs) (2004).
[8]R. E. P. Taylor, G. Yegin, and D. W. O. Rogers, "Benchmarking BrachyDose: Voxel-based EGSnrc Monte Carlo calculations of TG–43 dosimetry parameters," Med. Phys. **34**, 445–457 (2007).
[9]K. R. Russell, A. K. Carlsson-Tedgren, and A. Ahnesjö, "Brachytherapy source characterization for improved dose calculations using primary and scatter dose separation," Med. Phys. **32**, 2739–2752 (2005).
[10]J. F. Williamson, R. S. Baker, and Z. Li, "A convolution algorithm for brachytherapy dose computations in heterogeneous geometries," Med.

Phys. **18**, 1256–1265 (1991).
[11]A. K. Carlsson and A. Ahnesjö, "The collapsed cone superposition algorithm applied to scatter dose calculations in brachytherapy," Med. Phys. **27**, 2320–2332 (2000).
[12]A. K. Carlsson and A. Ahnesjö, "Point kernels and superposition methods for scatter dose calculations in brachytherapy," Phys. Med. Biol. **45**, 357–382 (2000).
[13]A. K. C. Tedgren and A. Ahnesjö, "Accounting for high Z shields in brachytherapy using collapsed cone superposition for scatter dose calculation," Med. Phys. **30**, 2206–2217 (2003).
[14]R. Wang and R. S. Sloboda, "Brachytherapy scatter dose calculation in heterogeneous media: I. A microbeam ray-tracing method for the single-scatter contribution," Phys. Med. Biol. **52**, 5619–5636 (2007).
[15]R. Wang and R. S. Sloboda, "Brachytherapy scatter dose calculation in heterogeneous media: II. Empirical formulation for the multiple-scatter contribution," Phys. Med. Biol. **52**, 5637–5654 (2007).
[16]G. Yegin, "A new approach to geometry modelling of Monte Carlo particle transport: an application to EGS," Nucl. Instrum. Methods Phys. Res. B **211**, 331–338 (2003).
[17]D. Baltas, P. Karaiskos, P. Papagiannis, L. Sakelliou, E. Loeffler, and N. Zamboglou, "Beta versus gamma dosimetry close to Ir-192 brachytherapy sources," Med. Phys. **28**, 1875–1882 (2001).
[18]R. Wang and X. A. Li, "Dose characterization in the near-source region for two high dose rate brachytherapy sources," Med. Phys. **29**, 1678–1686 (2002).
[19]P. Papagiannis, A. Angelopoulos, E. Pantelis, L. Sakelliou, D. Baltas, P. Karaiskos, P. Sandilos, and L. Vlachos, "Dosimetry comparison of ^{192}Ir sources," Med. Phys. **29**, 2239–2246 (2002).
[20]N. Patel, S. Chiu-Tsao, Y. Ho, T. Duckworth, J. A. Shih, H. Tsao, H. Quon, and L. Harrison, "High beta and electron dose from ^{192}Ir: implications for 'Gamma' intravascular brachytherapy," Int. J. Radiat. Oncol., Biol., Phys. **54**, 972–980 (2002).
[21]N. S. Patel, S.-T. Chiu-Tsao, J. A. Shih, Y. Ho, H.-S. Tsao, and L. B. Harrison, "Treatment planning dosimetric parameters for ^{192}Ir seed at short distances: Effects of air channels and neighboring seeds based on Monte Carlo study," Med. Phys. **31**, 1521–1528 (2004).
[22]J. Borg and D. W. O. Rogers, "Spectra and air-kerma strength for encapsulated ^{192}Ir Sources," Med. Phys. **26**, 2441–2444 (1999).
[23]M. J. Berger and J. H. Hubbell, XCOM: Photon cross sections on a personal computer, Report NBSIR87–3597, National Institute of Standards Technology (NIST), Gaithersburg, MD 20899, 1987.
[24]B. Duchemin and N. Coursol, "Reevaluation de l' ^{192}Ir," Technical Note LPRI/93/018, DAMRI, CEA, France (1993).
[25]D. Medich, M. Tries, and J. Munro, "Monte Carlo characterization of an ytterbium-169 high dose rate brachytherapy source with analysis of statistical uncertainty," Med. Phys. **33**, 163–172 (2006).
[26]J. Pérez-Calatayud, D. Granero, and F. Ballester, "Phantom size in brachytherapy source dosimetric studies," Med. Phys. **31**, 2075–2081 (2004).
[27]C. S. Melhus and M. J. Rivard, "Approaches to calculating AAPM TG–43 brachytherapy dosimetry parameters for ^{137}Cs, ^{125}I, ^{192}Ir, ^{103}Pd, and ^{169}Yb sources," Med. Phys. **33**, 1729–1737 (2006).
[28]F. Ballester, C. Hernandez, J. Pérez-Calatayud, and F. Lliso, "Monte Carlo calculations of dose rate distributions around ^{192}Ir wires," Med. Phys. **24**, 1221–1228 (1997).
[29]I. Kawrakow, "On the effective point of measurement in megavoltage photon beams," Med. Phys. **33**, 1829–1839 (2006).
[30]D. C. Medich and J. J. Munro, "Monte Carlo characterization of the M-19 high dose rate Iridium-192 brachytherapy source," Med. Phys. **34**, 1999–2006 (2007).
[31]J. F. Williamson and Z. Li, "Monte Carlo aided dosimetry of the microselectron pulsed and high dose-rate ^{192}Ir sources," Med. Phys. **22**, 809–819 (1995).
[32]R. E. P. Taylor and D. W. O. Rogers, "More accurate fitting of ^{125}I and ^{103}Pd radial dose functions," Med. Phys. **35**, 4242–4250 (2008).
[33]K. R. Russell and A. Ahnesjö, "Dose calculation in brachytherapy for a 192 Ir source using a primary and scatter dose separation technique," Phys. Med. Biol. **41**, 1007–1024 (1996).
[34]D. Granero, J. Perez-Calatayud, and F. Ballester, "Monte Carlo calculation of the TG-43 dosimetric parameters of a new BEBIG Ir-192 HDR source," Radiother. Oncol. **76**, 79–85 (2005).
[35]F. Ballester, J. Perez-Calatayud, V. Puchades, J. L. Lluch, M. A. Serrano-Andrés, Y. Limami, F. Lliso, and E. Casal, "Monte Carlo dosimetry of the Buchler high dose rate 192-Ir source," Phys. Med. Biol. **46**, N79–N90 (2001).
[36]F. Lliso, J. Perez-Calatayud, V. Carmona, F. Ballester, V. Puchades, and D. Granero, "Technical note: Fitted dosimetric parameters of high dose-rate ^{192}Ir sources according to the AAPM TG43 formalism," Med. Phys. **30**, 651–654 (2003).
[37]D. Granero, J. Perez-Calatayud, E. Casal, F. Ballester, and J. Venselaar, "A dosimetric study on the Ir-192 high dose rate Flexisource," Med. Phys. **33**, 4578–4582 (2006).
[38]F. Ballester, V. Puchades, J. L. Lluch, M. A. Serrano-Andrés, Y. Limami, J. Perez-Calatayud, and E. Casal, "Technical note: Monte-Carlo dosimetry of the HDR 12i and Plus ^{192}Ir sources," Med. Phys. **28**, 2586–2591 (2001).
[39]F. Ballester, V. Puchades, J. L. Lluch, M. A. Serrano-Andrés, Y. Limami, J. Perez-Calatayud, and E. Casal, "Erratum: Technical note: Monte-Carlo dosimetry of the HDR 12i and Plus ^{192}Ir sources [Med. Phys. **28**, 2586–2591 (2001)]," Med. Phys. **31**, 2372–2372 (2004).
[40]J. Perez-Calatayud, F. Ballester, M. Serrano-Andres, V. Puchades, J. Lluch, Y. Limami, and F. Casal, "Dosimetry characteristics of the Plus and 12i Gammamed PDR ^{192}Ir sources," Med. Phys. **28**, 2576–2585 (2001).
[41]P. Karaiskos, A. Angelopoulos, L. Sakelliou, P. Sandilos, C. Antypas, L. Vlachos, and E. Koutsouveli, "Monte Carlo and TLD dosimetry of an ^{192}Ir high dose-rate brachytherapy source," Med. Phys. **25**, 1975–1984 (1998).
[42]F. Lliso, J. Perez-Calatayud, V. Carmona, F. B. J. L. Lluch, M. A. Serrano, Y. Limami, and E. Casal, "Fitted dosimetric parameters of high dose-rate ^{192}Ir sources according to the AAPM TG43 formalism," Med. Phys. **28**, 654–660 (2001).
[43]F. Lliso, J. Perez-Calatayud, V. Carmona, F. B. J. L. Lluch, M. A. Serrano, Y. Limami, and E. Casal, "Erratum: Fitted dosimetric parameters of high dose-rate 192-Ir sources according to the AAPM TG43 formalism [Med. Phys. **28**(4), 654–660 (2001)]," Med. Phys. **28**, 1964–1964 (2001).
[44]P. Karaiskos, A. Angelopoulos, E. Pantelis, P. Papagiannis, L. Sakelliou, E. Kouwenhoven, and D. Baltas, "Monte Carlo dosimetry of a new ^{192}Ir pulsed dose rate brachytherapy source," Med. Phys. **30**, 9–16 (2003).
[45]G. M. Daskalov, E. Löffler, and J. F. Williamson, "Monte Carlo-aided dosimetry of a new high dose-rate brachytherapy source," Med. Phys. **25**, 2200–2208 (1998).
[46]G. M. Daskalov, "Erratum: Monte Carlo-aided dosimetry of a new high dose-rate brachytherapy source [Med. Phys. **25**, 2200–2208 (1998)]," Med. Phys. **27**, 1999–1999 (2000).
[47]R. Wang and R. S. Sloboda, "Monte Carlo dosimetry of the VariSource high dose rate 192-Ir source," Med. Phys. **24**, 415–423 (1998).
[48]P. Karaiskos, A. Angelopoulos, P. Baras, L. Sakelliou, P. Sandilos, K. Dardoufas, and L. Vlachos, "A Monte Carlo investigation of the dosimetric characteristics of the VariSource 192 Ir high dose rate brachytherapy source," Med. Phys. **27**, 1498–1592 (2000).
[49]A. S. Meigooni, M. T. Kleiman, J. L. Johnson, D. Mazloomdoost, and G. S. Ibbott, "Dosimetric characteristics of a new high-intensity ^{192}Ir source for remote afterloading," Med. Phys. **24**, 2008–2013 (1997).
[50]A. Angelopoulos, P. Baras, L. Sakelliou, P. Karaiskos, and P. Sandilos, "Monte Carlo dosimetry of a new ^{192}Ir high dose rate brachytherapy source," Phys. Med. Biol. **27**, 2521–2527 (2000).